journal

J. Am. Ceram. Soc., 96 [12] 3908–3914 (2013)
DOI: 10.1111/jace.12627

Flexural Strength by Fractography in Modern Brittle Materials

Roberto Dugnani[‡,†] and Ricardo Zednik[§]

[‡]University of Michigan – Shanghai Jiao Tong University Joint Institute, Shanghai, China

[§]Santa Clara University, Santa Clara, California 95053

Thin components made from advanced brittle glasses or ceramics are becoming increasingly important due to the widespread adoption of portable consumer products as well as other modern electronic and medical devices. The strength of these brittle materials is traditionally estimated from empirical relationships relating the stress at failure to characteristic lengths derived from the fracture surface's topography. One example is Orr's relationship, $\sigma_f \cdot R_m^{1/2} = A_m$, which correlates the material strength, σ_f, to the radius of the "mirror-mist boundary region," R_m, through the empirical constant, A_m. Although various studies have shown that, for flexural fractures (failed in bending), A_m depends on the specimen's geometry, this effect has been generally neglected by arguing that the magnitude of A_m is almost constant for thicker specimens. However, we show that this argument cannot be applied to thin geometries, and that by not accounting for the thickness of the sample, the flexural strength will be grossly underestimated. In this work, we introduce an expression based on an iterative fracture mechanics algorithm which yields more accurate estimates of flexural strength for thin brittle components in bending. The accuracy of the model is validated both through flexural strength tests on glass and by comparing our predictions to an extensive literature survey of experimental results.

I. Introduction

The increasing demand for smaller and lighter devices with a wide range of applications generates growing interest in the manufacturing of thin brittle components, such as glass screens, silicon chips, and ceramic resistors. For example, boro-silicate glasses (BSGs) as thin as 0.3 mm (Eagle™ XG slim; Corning, One Riverfront Plaza Corning, NY) for liquid crystal displays (LCD) and alumino-silicate glasses (ASGs) as thin as 0.5 mm (Gorilla™ 2; Corning) as cover glasses are becoming the norm in portable consumer products. It is also expected that the first consumer devices to use Corning's Willow™ Glass, a type of glass so thin (0.1 mm) and flexible that it can be rolled onto spools, will appear in 2013.[1]

The importance of thin brittle components highlights the necessity for an adequate means to estimate fracture strength. Unfortunately, most of the current tools are based on outdated models obtained from testing relatively thick bulk samples. In this manuscript, we propose and validate a fracture mechanics method that accounts for the sample thickness to estimate the fracture strength. Although the proposed model is consistent with Orr's equation for thick samples, it additionally provides an accurate prediction for thin geometries.

Our findings were validated by comparing predictions with extensive experimental flexural strength data from BSG, soda-lime glass (SLG) and ASG. These glasses are widely employed in electronic consumer products including television sets, laptop computers, smart phones, and tablets. The proposed model also applies to other brittle materials such as ceramics, single crystals, semicrystalline polymers, and glass-ceramics, as the form of the expressions used in the model's derivation are mechanism independent.

II. The Mirror Constant

The mirror-mist constant refers to the proportionality constant, A_m, first described by Orr's equation [Eq. (1)]. The value of the mirror constant is directly related to the crack tip's surface morphology during catastrophic crack growth. As cracks propagate during fracture, the surface roughness of the tip increases, as a progressively larger surface area is necessary to dissipate the potential strain energy stored in the material. When the crack tip's surface roughness approaches the wavelength of visible light, light is scattered by the fracture surface rather than being reflected. This optical interference effect causes the characteristic "hazy" or "misty" appearance at the boundary of the mirror-mist region.[2] The distance from the fracture origin to this hazy region is referred as the mirror radius, R_m. Figure 1 shows a schematic illustration of the mirror-mist transition on the surface of a glass fractured in flexure or bending. In Figs. 1(a) and (c) indicate the depth and the half-width of the crack at any given instant, respectively. The general convention for samples fractured in flexure or bending is to measure the mirror radius along the free surface of the plate on the tension side.

The strength of brittle materials is often estimated using well-established empirical relationships such as Orr's equation.[3] Orr showed that the magnitude of stress at failure, σ_f, is linearly correlated with the inverse of the square root of the mirror radius:

$$\sigma_f = \frac{A_m}{\sqrt{R_m}} \tag{1}$$

Figure 2 shows a plot of the average mirror constant, A_m, versus the thickness, H, of glass specimens as obtained by flexural strength tests conducted by various authors. Although the thickness of the sample is not accounted for in Eq. (1), the plot strongly suggests that a correlation might exist between A_m and the thickness H.

For the last half century, ceramists have tested and correlated the flexural strength of brittle materials with the corresponding lengths of the mirror radii, R_m, resulting in a rich literature. Generally, the mirror constant, A_m, is computed by fitting a linear function between the strength of the material and the inverse of the square root of the mirror radius as

M. Hoffman—contributing editor

Manuscript No. 33258. Received May 28, 2013; approved August 29, 2013.
[†]Author to whom correspondence should be addressed.
e-mail: roberto.dugnani@sjtu.edu.cn

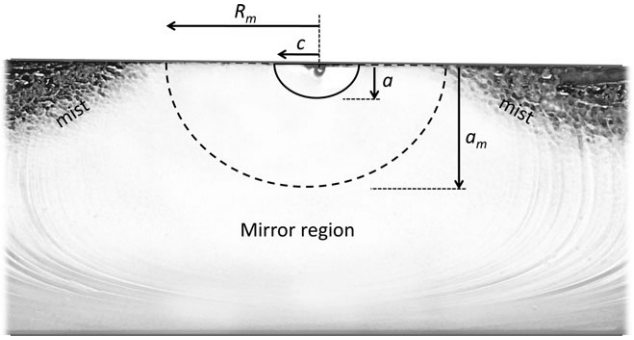

Fig. 1. Schematic view of mirror-mist radius, R_m, for a typical flexural fracture surface.

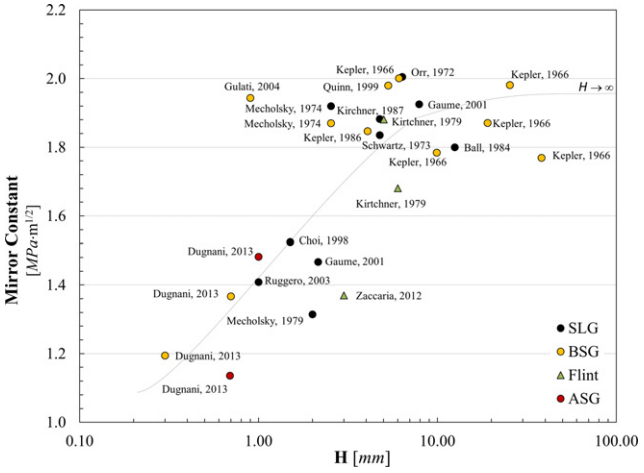

Fig. 2. Average mirror constant versus the thickness of the glass plates, H, as reported by various authors.

originally proposed by Orr.[3] However, various authors[4,5] noted that by introducing an additional fitting constant, $\Delta\sigma_0$, to Eq. (1), an improved fit to the experimental flexural strength data is obtained:

$$\sigma_f = \frac{A_m}{\sqrt{R_m}} + \Delta\sigma_o \tag{2}$$

The addition of the term $\Delta\sigma_o$ has often been justified by attributing it to "residual stresses" at the surface of the tested sample. Interestingly, $\Delta\sigma_o$ is almost always reported as a positive term, indicating "tension." Nonetheless, the presence of tension stresses at the glass surface is inconsistent with the glass-forming process which predicts compressive stresses at the surface prior to annealing. We propose an alternative explanation where the mirror constant, A_m, is a function of the sample thickness and the term $\Delta\sigma_o$ corresponds to the residual surface stress only in the case of thick specimens.

(1) The Mirror Constant's Magnitude

In the past, various studies showed that the magnitude of the mirror constant, A_m, is related to material properties as well as the dimensions of the sample. For instance, Mecholsky *et al.*[6] gives an equation for the mirror constant relating its value to the critical stress intensity of the material, K_{Ic}, the ratio of the initial flaw radius to the mirror radius, c_o/R_m, and the shape factor for the initial flaw, Y_0. Mecholsky *et al.*,[7] also showed that for thick samples the ratio c_o/R_m is almost equal to the fractal number, D^*. Hence, based on these two works:

$$A_m = \frac{Y_o}{\sqrt{2}} \frac{K_{IC}}{(c_o/R_m)^{1/2}} = \frac{Y_o}{\sqrt{2}} \left(\frac{Y_0}{Y_{0m}}\right)^{1/4} \frac{K_{IC}}{D^{*1/2}} \tag{3}$$

The fractal number, D^*, in Eq. (3) describes the degree of tortuosity of the fracture surface and its value is relatively constant. The term Y_0/Y_{0m} is the ratio of the shape factor of the initial flaw over the crack's shape factor at the onset of the mist region. As shape factors are related to the geometry of the sample, it follows that the mirror constant, A_m, must also depend on the glass thickness, H.

III. Stress Intensity and Mist Formation

The quasi-static stress intensity factor (SIF), K_I, is generally defined as the product of the far-field stress multiplied by the square root of the crack depth, a, times the shape factor Y, a term introduced to account for the uneven stress distribution at the crack boundary. The shape factor, Y, is a function of the crack's shape, the sample's geometry, and distribution of the stress field applied to the specimen. Shape factors for static loading have been computed by various authors for numerous crack shapes and loading scenarios.[8] The value of the shape factor at the onset of the mirror, Y_{0m}, is of particular interest, as various authors[9] suggest that mist formation is linked to a particular value of the SIF, K_{Im}. Hence, the quasi-static SIF at the onset of the mist region can be expressed as follows:

$$K_{Im} = Y_{0m}\sigma_f \sqrt{a_m} \tag{4}$$

The term a_m in Eq. (4) refers to the depth of the crack at the instant when the half-width of the crack is equal to the mirror radius, R_m. Note that although the mist appears at R_m, no mist is necessarily present at a_m, as the stress intensity is not constant along the crack front.[7] Combining Eqs. (4) and (1), we obtain a relationship describing A_m as a function of K_{Im}, the geometric factor Y_{0m}, and the square root of the ratio R_m/a_m:

$$A_m = \frac{K_{Im}}{Y_{0m}} \sqrt{\frac{R_m}{a_m}} \tag{5}$$

As it will be shown in later in this study, Eq. (5) provides the means to estimate the value of the SIF at the onset of the mist region, K_{Im}.

IV. Crack Evolution Model

The value of the mirror constant, A_m, is a function of the crack shape at the onset of the mist region as shown in Eq. (3). To calculate the mirror constant, A_m, the crack shape during fast-growth first needs to be calculated and subsequently used to evaluate the shape factor, Y_{0m}. We employ a numerical algorithm based on fracture mechanics principles to estimate the evolution of the crack shape as it propagates into a sample of constant thickness, H. A schematic block diagram describing the steps involved in this iterative crack evolution model is shown in Fig. 3. The algorithm used in this work combines both the works of Dwivedi and Green[10] for subcritical crack growth with the work of Sharon and Fineberg[11] for fast propagating cracks.

The evolution of the crack shape can be divided into two distinct regimes, depending on the factors driving the growth: the subcritical range is driven by environmental factors such as moisture, whereas the fast crack range is driven by the strain energy release rate. The evolution of the crack shape in both regimes can be determined from a marching time numerical algorithm provided that the stress profile, the initial geometry of the specimen, and the crack tip velocity are

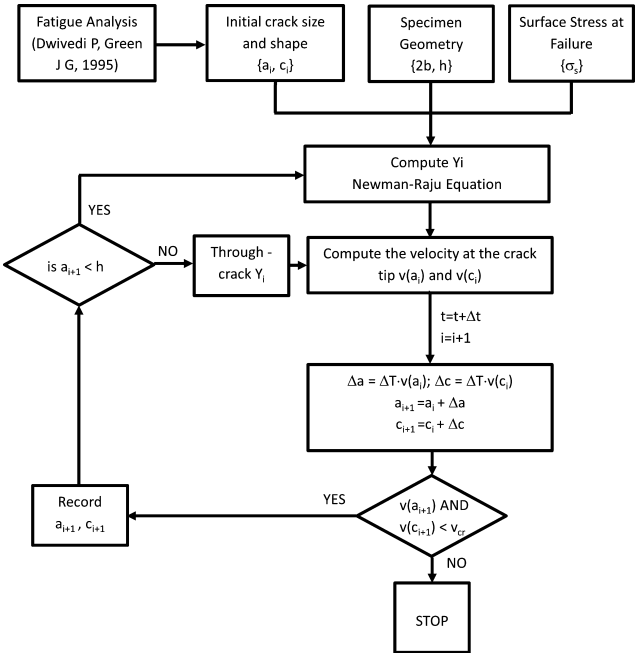

Fig. 3. Block diagram for crack shape evolution algorithm.

known. In the proposed model the tested samples are monotonically loaded in bending. The original flaw therefore initially propagates in the subcritical growth range until K_I reaches the critical value for the material, K_{Ic}. As soon as $K_I = K_{Ic}$, the crack is assumed to be driven by the strain energy release rate.

The crack growth model for subcritical crack growth has been developed and validated by Dwivedi and Green.[10] The crack velocity for the subcritical crack growth region can be described by the equation:

$$v = v_s \left(\frac{K_I}{K_{Ic}}\right)^n \quad \text{for} \quad K_I < K_{Ic} \tag{6}$$

In this study, $n = 20$ and $v_s = 0.26$ mm/s, based on typical SLG values reported by Dwivedi *et al.*[10]

For fast propagating cracks, the crack tip velocity, v, correlates with the square of the critical SIF over the local SIF[10,11] [Eq. (7)], where c_R represents the Raleigh speed. Observations by numerous authors indicate that the speed of the crack tip practically only reaches a maximum speed, v_{max}, of less than half its theoretical c_R value. Hence, the velocity of the crack tip can be approximated by the equation:

$$v = c_R\left(1 - \frac{K_{Ic}^2}{K_{Id}^2}\right) \text{for } v < v_{max} (\approx c_R/2) \tag{7}$$

Equation 7 is a variation of Freund[12] equation of motion where the SIF instead of the energy release rate is used in the computation of the crack speed. The term K_{Id} in Eq. (7) stands for the dynamic SIF. K_{Id} is related to the static SIF using test data for SLG reported by Sharon and Fineberg.[11] The values of c_R and v_{max} used in this work are also based on the experimental data reported by Sharon *et al.*,[11] i.e., $c_R = 3300$ m/s, and $v_{max} = 1550$ m/s. Quinn[5] and Swartz[13] also report similar values.

For the fast crack regime, the Newman and Raju[8] equations are used to determine the quasi-static shape factor at the crack's tip along the principal axis (i.e., Y_0 and Y_{90}). These values are then used to calculate the corresponding dynamic SIF. Based on this SIF calculation, the extensions of the crack along the principal axes of the elliptical crack are computed as $\Delta a = v_{90}\cdot\Delta T$ and $\Delta a = v_{90}\cdot\Delta T$, respectively, where the crack speed is obtained based on either Eqs. (6)) or (7) depending on whether the crack is propagating in the subcritical range ($K_I < K_{Ic}$) or in the fast crack range ($K_I \geq K_{Ic}$). For the fracture of brittle plates in bending, the crack shape is assumed semielliptical until the crack front reaches the depth $a = 0.8\cdot H$. Experiments conducted by Sherman and Be'ery.[14] on SLG plates indicate that, for flexural tests, the crack does not grow into the depth direction as $a = 0.8\cdot H$, but rather propagates longitudinally while maintaining a constant crack front shape.

A final remark should be made about how the formation of mist and corresponding length of the mirror radius, R_m, was determined in our numerical algorithm. Various authors suggested that the mist forms at the crack tip as the SIF reaches K_{Im}. For convenience in the numerical code, we calculated the onset of the mist region based on the velocity of the crack tip rather than K_{Im}. Based on Eq. (7), the value of K_{Im} uniquely defines the velocity of the crack tip, v_m, at the onset of the mist, and hence the two criteria are equivalent. In particular, for a value of the mist SIF, $K_{Im} = 2.3$ MPa·m$^{1/2}$ and $K_{Ic} = 0.75$ MPa·m$^{1/2}$, the velocity of the crack as mist forms is predicted by Eq. (7) as $v_m \approx 0.5\ c_R$, which is consistent with the reported velocity at the onset of the mist region from previous studies.[15]

V. Four-Point Bending Tests

To determine the appropriate value of the mirror constant A_m for thin glasses, four-point bending (4PTB) tests were carried out on thin rectangular glass samples. After all samples had been tested, the fracture surface for each sample was inspected by optical microscopy and the dimension of the mirror radius, R_m, determined according to ASTM C1256.[16] 4PTB tests were conducted on ASG (140 samples each 0.98 mm thick, 28 samples each 0.69 mm thick) and BSG (35 samples each 0.71 mm thick and 12 samples each 0.32 mm thick). Neither edge treatment nor annealing was performed on the samples prior to testing. The test setup and loading rate (1.1 ± 0.1 MPa/s), as well as the fixture dimensions were selected based on recommendations outlined in ASTM Standard C158-02.[17] All tests were carried out on an Instron universal pull tester with a load cell resolution of 0.01 N. As prescribed by ASTM C158-02, the flexural strength was computed as follows:

$$\sigma_f = \frac{3Ld}{bH^2} \tag{8}$$

where L describes the breaking load, d is the moment arm or distance between adjacent supports and loading edges, b is the width of the specimen, and H is the thickness of the specimen. All samples that broke at the rollers were rejected. Equation (8) is valid for small displacements only. For large displacement corrections are generally applied to predict the correct stress at failure. For instance, ASTM Standard D790-02[18] considers what correction should be applied to the stress equation if the beam experiences large deflections (greater than 10% of the support span). In this work, the fracture strength was computed by finite element analysis software to include the nonlinear effects due to the large deflections.

VI. Results

In an effort to better understand the relationship between the mirror radius and the flexural strength of a material fractured in bending, a numerical fracture mechanics model that incorporates sample thickness dependence to predict the mist formation was developed. In this section, we describe the results obtained from testing thin BSG and ASG by 4PTB tests, and augment our experimental data with results

collated from the literature. Overall, the data analyzed include mirror radii and flexural strength measurements from glass specimens with thicknesses ranging from 0.3 to 38 mm. Table I compares the fitting constants computed using Orr's equation to our proposed fit for the results obtained from various experimental studies.

To understand the effects of sample thickness, simulations based on the crack evolution algorithm are carried out for various values of H and initial flaw sizes. For each simulation, a pair of flexural strength and mirror radius is obtained. Repeating this process for a broad set of flaw sizes conditions allows us to obtain trends relating the strength of the glass to the inverse of the square root of the mirror radius for various values of H. The data obtained is found to collapse onto a one single curve described by Eq. (9):

$$\sigma_f = \frac{K_{Im}\left[2.02 - 1.20\exp\left(-0.459\frac{R_m}{H}\right)\right]}{\sqrt{R_m}} = \frac{A_{md}(R_m/H)}{\sqrt{R_m}} \tag{9}$$

The numerator of Eq. (9) defines a "dynamic" mirror coefficient, A_{md}, which, unlike A_m in Orr's equation, is a function of the ratio between the mirror radius and the thickness of the sample. In the spirit of including the effects of residual stresses, a constant $\Delta\sigma_d$, analogous to $\Delta\sigma_o$ of Eq. (2) was added to Eq. (9):

$$\sigma_f = \frac{A_{md}(R_m/H)}{\sqrt{R_m}} + \Delta\sigma_d \tag{10}$$

Table I shows that for all the data considered, the mirror constant, A_m, ranges from 1.14 to 2.23 MPa·m$^{1/2}$, whereas K_{Im} ranges from 1.77 to 2.81 MPa·m$^{1/2}$. Based on the data available, it was found that $K_{Im} = 2.29 \pm 0.15$ MPa·m$^{1/2}$ ($N = 213$) resulted in the best fit for SLG, $K_{Im} = 2.38 \pm 0.19$ MPa·m$^{1/2}$ for BSG ($N = 331$), $K_{Im} = 2.30 \pm 0.15$ for ASG glass ($N = 168$), and $K_{Im} = 2.11 \pm 0.14$ MPa·m$^{1/2}$ for flint glass ($N = 13$). The SIF at the onset of the mist region, K_{Im}, is found to be independent of the specimen's thickness H. Conversely, the magnitude of the mirror constant, A_m, generally increases as H increases, as shown in Fig. 2.

In addition, the residual stresses obtained using Eq. (10), $\Delta\sigma_d$, are often negative (i.e., compression), whereas Orr's relationship predicts positive values (i.e., tension) for $\Delta\sigma_o$ in all cases. The average residual stresses predicted by Orr's relationship based on the data analyzed is about 20 MPa, whereas using the proposed model the average value is approximately −6 MPa. Finally, the residual stress based on Orr's model, $\Delta\sigma_o$, increases as H decreases, whereas no correlation is found between $\Delta\sigma_d$ and H. The "residual stresses" predicted by Orr's relationship therefore appear, for the most part, to be a mismatch artifact caused by the simplified fitting equation.

Figure 4 shows a plot for A_{md}/K_{Im} versus R_m/H for over 770 fractured specimens obtained both from the literature[3,9,12,19,20,20–29] and tests conducted by the authors. It should be noted that Zaccaria and Overend[30] data for flint glass flexural strength was omitted in the plot as well as in the calculations of K_{Im}. As Zaccaria's manuscript did not report the fixture span used in their 4PTB, it was not possible to independently verify whether a corrections for large deflection in the fracture strength calculations should have been applied to this set of data. In this analysis, mirror radii larger than 20% of the sample's width are omitted as the crack-evolution model described in the previous section assumes an infinite sample width and finite sample thickness. SLG, ASG, and BSG are all shown on the same plot as the values of K_{Im} are similar for the three cases. For reference, Fig. 4 also shows the trend from the numerical algorithm

Table I. Summary of Fitting Constants and Test Conditions for Flexural Strength Data on Boro-Silicate (BSG), Soda-Lime (SLG), Alumino–Silicate (ASG), and Flint Glass

			Orr's equation		Proposed fit			
Author	Glass type	H (mm)	A_m (MPa√m)	$\Delta\sigma_o$ (MPa)	K_{Im} (MPa√m)	$\Delta\sigma_d$ (MPa)	Samples tested	Test conditions
Dugnani	BSG	0.3	1.19	88.0	2.18 ± 0.16	−0.7	35	4PBT
Dugnani	BSG	0.7	1.37	31.6	2.26 ± 0.12	−21.4	12	4PBT
Dugnani	ASG	0.7	1.14	35.0	1.88 ± 0.05	−12.1	28	4PTB
Gulati[19]	BSG	0.9	1.94	11.9	2.63 ± 0.08	−25.5	32	RoR
Dugnani	ASG	1.0	1.48	34.1	2.37 ± 0.15	−15.6	140	4PTB
Ruggero[20]	SLG	1.0	1.41	15.0	2.06 ± 0.12	−22.7	41	4PTB, annealed
Choi and Gyekenyesi[21]	SLG	1.5	1.52	13.4	1.77 ± 0.27	0.0	12	RoR, annealed
Mecholsky *et al.*[22]	SLG	2.0	1.31	18.4	2.34 ± 0.16	−19.5	22	4PTB
Gaume and Pelletier[23]	SLG	2.2	1.47	19.5	1.90 ± 0.17	0.0	24	4PTB
Mecholsky and Rice[24]	BSG/Silicate	2.5	2.13	8.7	2.62 ± 0.43	−6.9	21	RoR
Zacaria and Overend[30]	Flint Glass	3.0	1.37	11.0	n/a	n/a	33	4PTB
Kerper and Scuderi[25]	BSG	4.1	1.85	16.6	2.48 ± 0.16	−2.4	22	Flexure, rods
Schwartz[13]	SLG	4.8	1.84	10.3	2.53 ± 0.19	−9.3	25	4PTB, annealed
Kirchner and Conway[26]	SLG	4.8	1.88	10.1	1.88	2.7	2	Flexure, rods
Kirchner and Kirchner[9]	Flint	5.0	1.88	25.0	2.09 ± 0.16	26.3	25	Flexure, rods
Quinn[27]	BSG	5.3	1.98	9.6	2.60 ± 0.12	−5.0	45	RoR, Annealed
Kirchner and Kirchner[9]	Flint	6.0	1.68	24.7	2.16 ± 0.10	11.2	13	Flexure, rods
Kerper and Scuderi[25]	BSG	6.1	2.00	7.0	2.51 ± 0.16	0.3	20	Flexure, rods
Orr[3]	SLG	6.4	2.01	4.1	2.81 ± 0.05	−12.8	46	RoR
Gaume and Pelletier[23]	SLG	7.9	1.92	6.9	2.22 ± 0.29	0.0	25	4PTB
Kerper and Scuderi[25]	BSG	9.9	1.78	8.1	2.17 ± 0.14	4.9	25	Flexure, rods
Shand[28]	BSG	11.6	2.23	35.1	2.59 ± 0.19	0.0	19	4PTB, annealed rods
Ball *et al.*[29]	SLG	12.5	1.80	1.4	2.11 ± 0.11	0.3	16	3PTB, annealed
Kerper and Scuderi[25]	BSG	19.1	1.87	7.1	2.13 ± 0.27	8.4	63	Flexure, rods
Kerper and Scuderi[25]	BSG	25.4	1.98	6.9	2.53 ± 0.17	2.2	39	Flexure, rods
Kerper and Scuderi[25]	BSG	38.1	1.77	9.1	2.28 ± 0.25	4.8	39	Flexure, rods

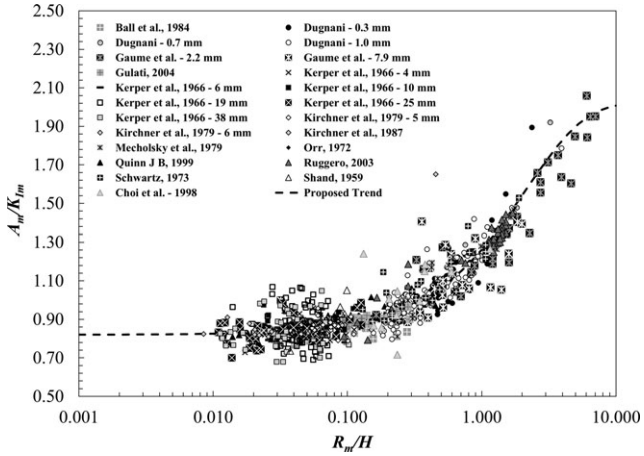

Fig. 4. A_m/K_{Im} versus R_m/H for $N = 770$ glass samples fractured in bending.

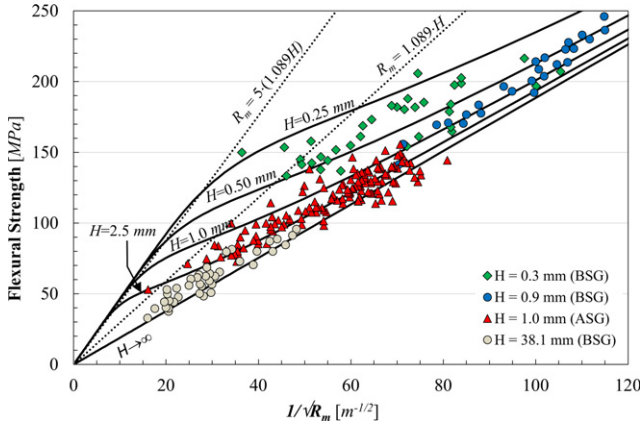

Fig. 5. Expected glass strength versus $1/\sqrt{R_m}$ for $H = 0.25$, 0.5, 1.0, and 2.5 mm, and $H \to \infty$ (solid lines, $K_{Im} = 2.3$ MPa·$m^{1/2}$). Also shown are flexural strength data for $H = 0.3$, 0.9, 1, and 38.1 mm.

described by Eq. (10). The data from the literature and the predictions from our model are in excellent agreement. The large spread of the strength/mirror radius is associated with the variation in the strength due to the statistical nature of strength in brittle materials.

Figure 5 shows a plot of the predicted flexural strength based on Eq. (10) versus $1/\sqrt{R_m}$ for H =0.25, 0.5, 1, 2.5 mm and $H \to \infty$ for a value of $K_{Im} = 2.3$ MPa·$m^{1/2}$. Also on the same plot are shown data from selected flexural strength tests conducted on samples with thicknesses ranging from 0.3 to 38.1 mm. The experimental trend is in good agreement with the behavior predicted by Eq. (10). It is clear that, for thicker glasses (i.e., $H > 2.5$ mm), Eq. (10) and Orr's equation ($H \to \infty$) yield almost identical predictions.

VII. Discussion

In this section, we provide a method for estimating the values of K_{Im} for isotropic brittle materials based on tensile test data. In addition, we also discuss the limitations of Orr's equation and give recommendations regarding the broader applicability of the proposed model [Eq. (10)].

(1) Estimating K_{Im}

The proposed expression for flexural strength prediction shown in Eq. (10) can be easily implemented as long as the value of K_{Im} for the material considered is known. However, for most brittle materials, this parameter is not readily available in the literature. Nonetheless, Eq. (5) provides a relatively simple way to estimate K_{Im} for brittle, isotropic materials.

For a thick plate (i.e., $a_m << H$) in bending, or for any sample tested in tension, the most likely shape of the initial flaw after subcritical crack growth is $a_o/c_o = 0.85$ as shown by Dwivedi *et al.*[10] A survey conducted on numerous fractured ASG samples[31] also confirmed that $a_0/c_0 \approx 0.8$. For tensile tests on large specimens (or flexural tests on thick samples), the shape of the flaw will not change substantially during growth; hence, K_{Im} can be estimated from Eq. (5), assuming $a_m/R_m = 0.85$ and $Y_{0m} \approx 1.3$. This yields a simple expression for estimating K_{Im}:

$$K_{Im} \approx 1.2 \cdot A_{m,T} \tag{11}$$

$A_{m,T}$ in Eq. (11) refers to the mirror constant obtained from tension tests, which are more common in the literature. For instance, using the value $A_{m,T} = 1.72 \pm 0.28$ MPa·$m^{1/2}$ for SLG[32] and $A_{m,T} = 1.9$ MPa·$m^{1/2}$ for BSG,[33] K_{Im} can be estimated as 2.1 MPa·$m^{1/2}$ (SLG) and 2.3 MPa·$m^{1/2}$ (BSG).

(2) The Mirror Behavior

Figure 4 shows a plot of the "dynamic" mirror coefficient, A_{md}, normalized by K_{Im} versus the ratio R_m/H. A_{md} has two asymptotic values corresponding to "infinitely small" and "infinitely large" values of H. The first part of our discussion focuses on the expected asymptotic behavior of A_{md} for the two cases of very thin and very thick specimens. Two different approaches can be used to calculate the behavior of the mirror coefficient in these limiting cases.

The first approach used to investigate the behavior for the dynamic mirror constant, A_{md}, employs Eq. (5). For the infinitely thick sample case, we expect the crack aspect ratio at the onset of the mirror region, $R_m/a_m \approx 1.25$ and hence $Y_{0m} = 1.3$. Substituting into Eq. (5), and assuming an average value of $K_{Im} = 2.4$ MPa·$m^{1/2}$ for SLG and BSG, the dynamic mirror coefficient $A_{md} \approx 2.1$ as $H \to \infty$. This value is in good agreement with reported values for the mirror constant found in the literature for tests in tension indicating $A_{m,T} = 1.72$ MPa·$m^{1/2}$ (SLG)[32] and 1.9 MPa·$m^{1/2}$ (BSG).[33] For thin samples, the effective crack's aspect ratio R_m/a_m is ~3.125 based on observations made by Sherman *et al.*[10] and hence $Y_{0m} \approx 1.1$. Substituting into Eq. (5) yields the dynamic mirror coefficient $A_{md} = 3.3$ as $H \to 0$. These analytical asymptotic values based on Eq. (5) are in reasonable agreement with the values expected from the crack evolution model.

A second approach to estimate the value of the dynamic mirror coefficient, A_{md}, for the case of a thick sample is using Eq. (3). As for thick samples Eq. (10) trends to Orr's equation because $A_m = A_{md}$ as $H \to \infty$, it follows that Eq. (3) can be used to study the asymptotic behavior of the mirror coefficient. Taking the limit of Eq. (3) for an infinitely thick sample, the mirror constant, A_m, can be expressed as follows:

$$\lim_{H\to\infty} A_m = \lim_{H\to\infty} A_{md} = K_{IC}\frac{Y_0}{\sqrt{2}(c_o/R_m)^{1/2}} \approx \frac{K_{IC}\,Y_0}{\sqrt{2D^*}} \tag{12}$$

For an infinitely thick sample, the most likely shape for the initial flaw after subcritical crack growth is $a/c = 0.85$, as shown by Dwivedi *et al.*,[10] corresponding to $Y_0 \approx 1.3$. Various studies estimate the fractal exponent D^* for SLG[7] ($D^* = 0.08$), BSG[7,34] ($D^* = 0.07$–0.10) and ASG[7] ($D^* = 0.08$). In all cases, only thick samples were considered in the estimation of D^*. Assuming a value for the critical strength intensity factor $K_{Ic} = 0.7$–0.75 MPa·$m^{1/2}$ for BSG, SLG, and ASG, it follows based on Eq. (11) that $A_{md}|_{H \to \infty} = 2.0$–$2.6$ MPa·$m^{1/2}$. This range is in agreement with the prediction

of Eq. (5). More accurate measurements for D^* would be required to improve the estimate. Since D^* are similar for the types of glass considered, based on Eqs. (10) and (12), we should also expect K_{Im} to have similar magnitudes. This observation is consistent with the results from the previous section, which indicate almost identical values of K_{Im} for the types of glass considered.

Figure 5 shows that Orr's equation can accurately describe the behavior of the system for thick glasses in bending (i.e., $H > 2.5$ mm). Nonetheless, Orr's equation becomes more and more inaccurate for $H < 2.5$ mm, especially for larger values of R_m. Equations (13) and (14) give the first and second derivatives of Eq. (10) with respect to $(1/\sqrt{R_m})$:

$$\frac{\partial \sigma_f}{\partial(1/\sqrt{R_m})} = K_{Im}\left\{2.02 - 1.2\exp\left(-0.459\frac{R_m}{H}\right)\cdot\left[1 + 0.918\frac{R_m}{H}\right]\right\} \tag{13}$$

$$\frac{\partial^2 \sigma_f}{\partial(1/\sqrt{R_m})^2} = -1.016\frac{R_m}{H}\sqrt{R_m}\exp\left(-0.459\frac{R_m}{H}\right)\cdot\left[0.918\frac{R_m}{H-1}\right] \tag{14}$$

The first derivative [Eq. (13)] can be thought of as the local value of the mirror constant for a given glass thickness and mirror radius. Near the origin of the axes (i.e., for $1/\sqrt{R_m} \to 0$) the slope of the curve is the steepest and its magnitude has a value of $2.02K_{Im}$. The slope decreases as $1/\sqrt{R_m}$ increases up until the inflection point (i.e., second derivative equals zero) is reached. Past the inflection point, the slope of the curve slowly increases and its value tends to the asymptotic value of $0.81K_{Im}$.

As seen in Fig. 5, most of the strength data available from the literature fall in the region past the inflection point where the slope of the strength versus $1/\sqrt{R_m}$ is almost constant. In this region, a linear fit as the one proposed by Orr's equation generally describes the behavior of the curve but it inevitably results in a positive intercept with the ordinate axis. This effect is more obvious for thinner samples. As expected, thicker samples require a higher positive intercept with the ordinate axis when fitted using Orr's equation. All data analyzed are in the range $R_m/H < 7$, as the literature does not report experimental results for very thin, low strength glasses.

To obtain the value of the inflection point, Eq. (14) can be set equal to zero, which leads to the equation, $R_m = 1.089H$. For values of $1/\sqrt{R_m}$ to the right of the inflection point (i.e., $R_m < 1.089H$) the slope of the strength versus $1/\sqrt{R_m}$ curve changes gradually and Orr's equation might be used accurately as long as the intercept $\Delta\sigma_o$ is either kept small ($H < 2.5$ mm) or is known from testing. For approximate values of the mirror radius such that $R_m > 5 \cdot (1.089H)$, the slope of the curve changes dramatically as shown in Fig. 5. It follows that flexural strength data in the approximate range $1.089H < R_m < 5 \cdot (1.089H)$ are likely to fit Orr's linear equation rather poorly. A typical flexural strength of 70 MPa corresponds to a mirror radius of ~0.75 mm, and falls in the nonlinear range of the strength versus $1/\sqrt{R_m}$ curve for values of H between 0.15 and 0.75 mm.

VIII. Conclusions

In this study, we show that the radius of the mirror region obtained from brittle bending fractures is a function of the sample thickness, H. A new relationship to estimate the flexural strength of samples using fractographic measurements that include the effect of H is proposed. This has important implications for modern devices in a wide range of industries, where advanced brittle materials in thin geometries are becoming increasingly common.

Although previous models based on Orr's equation are reasonably accurate for $H > 2.5$ mm, it is found that for $H < 2.5$ mm the linear fit suggested by Orr needs to be offset by a phenomenological stress fitting constant, $\Delta\sigma_o$, which is not compatible with stress states typically observed in thin components; although our approach does not necessarily require such adjustments, an analogous $\Delta\sigma_d$ term that better represents the underlying residual stress can be included if desired. In this work, we also describe a simple method for estimating K_{Im} in brittle isotropic materials based on traditional tension tests that are more readily available in the literature.

Our approach is based on a general fracture mechanics crack evolution framework that is applicable to any brittle system. As an example to verify the validity of our model, we applied it to data available from flexural strength tests on SLG, ASG, and BSG. Flexural data from SLG, ASG, and BSG indicate that a single fitting parameter, i.e., the static SIF at the onset of the mist region, K_{Im}, can be used to reasonably predict the strength of glass based on the mirror radius measurements.

References

[1]Corning Website, Corning Willow Glass: Fact Sheet, http://www.corning.com/WorkArea/showcontent.aspx?id=51335, 26 April, 2013.

[2]D. Hull, "Influence of Stress Intensity and Crack Speed on Fracture Surface Topography: Mirror to Mist Transition," *J. Mater. Sci.*, **3**, 1829–41 (1996).

[3]L. Orr, "Practical Analysis of Fractures in Glass Windows," *Mater. Res. Stan.*, **12** [1] 21–3 (1972).

[4]J. C. Conway and J. J. Mecholsky, "Use of Crack Branching Data for Measuring Near-Surface Residual Stresses in Tempered Glass," *J. Am. Ceram. Soc.*, **72** [9] 1584–7 (1989).

[5]G. D. Quinn, "Guide to Practice for Fractography of Ceramics and Glasses"; NIST Special Publication SP 960-16, Washington, May, 2007.

[6]J. J. Mecholsky, S. W. Freimam, and R. W. Rice, "Fracture Surface Analysis of Ceramics," *J. Am. Ceram. Soc.*, **11** [7] 1310–9 (1976).

[7]J. J. Mecholsky and S. W. Freiman, "Relationship between Fractal Geometry and Fractography," *J. Am. Ceram. Soc.*, **75** [12] 3136–8 (1991).

[8]J. C. Newman and I. S. Raju, "An Empirical Stress-Intensity Factor Equation for the Surface Crack," *Eng. Fract. Mech.*, **15** [1–2] 185–92 (1981).

[9]H. P. Kirchner and J. W. Kirchner, "Fracture Mechanics of Fracture Mirrors," *J. Am. Ceram. Soc.*, **62** [3–4] 198–202 (1979).

[10]P. Dwivedi and D. J. Green, "Indentation Crack-Shape Evolution during Subcritical Crack Growth," *J. Am. Ceram. Soc.*, **78** [5] 1240–6 (1995).

[11]E. Sharon and J. Fineberg, "Confirming the Continuum Theory of Dynamic Brittle Fracture for Fast Cracks," *Nature*, **397**, 333–5 (1999).

[12]L. B. Freund, *Dynamic Fracture Mechanics*. Cambridge University Press, Cambridge, UK, 1990.

[13]T. A. Schwartz, "The Fractography of Inorganic Glass"; M.Sc. Thesis, MIT, Boston, 1977.

[14]D. Sherman and I. Be'ery, "Shape and Energies of a Dynamically Propagating Crack under Bending," *J. Mater. Res.*, **18** [10] 2379–86 (2003).

[15]H. G. Richter and F. Kerkhof, *Fractography of Glass*. Plenum, New York, 1994.

[16]ASTM C1256-93, "Standard Practice for Interpreting Glass Fracture Surface Features", ASTM International, West Conshohocken, PA, 2008.

[17]ASTM C158-02, "Standard Test Methods for Strength of Glass by Flexure (Determination of Modulus of Rupture)"; ASTM International, West Conshohocken, PA, 2007.

[18]ASTM D790-02, "Standard Test Methods for Flexural Properties of Unreinforced Plastics and Electrical Insulating Materials"; ASTM International, West Conshohocken, PA, 2002.

[19]S. T. Gulati, J. F. Bayne, W. R. Powell, and J. D. Helfinstine, "Mirror Constant for AMLCD Glass," *Am. Ceram. Soc. Bull.*, **83** [5] 9301–3 (2004).

[20]A. A. Ruggero, "Quantitative Fracture Analysis of Etched Soda-Lime Silica Glass: Evaluation of Blunt Crack Hypothesis"; M.Sc. Thesis, University of Florida, 2003.

[21]S. R. Choi and J. P. Gyekenyesi, "*Crack Branching and Fracture Mirror Data of Glasses and Advanced Ceramics*"; NASA-TM-1998-206536, 1998.

[22]J. J. Mecholsky, A. C. Gonzalez, and S. W. Freiman, "Fractographic Analysis of Delayed Failure in Soda-Lime Glass," *J. Am. Ceram. Soc.*, **62** [11–12] 577–80 (1979).

[23]O. Gaume and S. Pelletier, "Analysis of Fracture Features for uni-Axial Bent Glass Plates," Saint-Gobain Recherche, Technical Document, April 26, 2013. http://kdsolution.com/pdf_upload/Gaume.pdf

[24]J. J. Mecholsky and R. W. Rice, *Fractographic Analysis of Biaxial Failure in Ceramics*. American Soc. for Testing and Materials, West Conshohocken, PA, STP 827, 1984.

[25]M. J. Kerper and T. G. Scuderi, "Relation of Fracture Stress to the Fracture Pattern for Glass Rods of Various Diameters," *Bull. Am. Ceram. Soc.*, **45** [12] 1065–6 (1966).
[26]H. P. Kitchner and J. C. Conway, "Comparison of the Stress-Intensity and Johnson-and-Holloway Criteria for Crack Branching in Rectangular Bars," *J. Am. Ceram. Soc.*, **70** [8] 565–9 (1987).
[27]J. B. Quinn, "Extrapolation of Fracture Mirror and Crack-Branch Sizes to Large Dimensions in Biaxial Strength Tests of Glass," *J. Am. Ceram. Soc.*, **82** [8] 2126–32 (1999).
[28]E. B. Shand, "Breaking Stress of Glass Determined From Dimensions of Fracture Mirrors," *J. Am. Ceram. Soc.*, **42** [10] 474–7 (1959).
[29]M. J. Ball, D. J. Landini, and R. C. Bradt, "Fracture Mist Region in a Solda-Lime-Silica Float Glass"; pp. 110–20 in *Fractography of Ceramic and Metal Failures*, ASTM STP 827, Edited by J. J. Mecholsky Jr. and S. R. Powell Jr. American Society for Testing and Materials, West Conshohocken, PA, 1984.
[30]M. Zaccaria and M. Overend, "Validation of a Simple Relationship Between the Fracture Pattern and the Fracture Stress of Glass"; Engineered Transparency. pp. 1–9 in International Conference at Glasstec, Düsseldorf, Germany, October 25-26, 2012.
[31]R. Dugnani, Z. Pan, and M. Wu, "Degradation of Consumer Products Glasses after Extended Use," *2009 MS&T Proc.*, **1**, 500–9 (2009).
[32]A. I. A. Abdel-Latif, R. C. Bradt, and R. E. Tressler, "Dynamics of Fracture Mirror Boundary Formation in Glass," *Int. J. Fract.*, **13** [3] 349–59 (1977).
[33]O. E. Alarcon, R. E. Medrano, and P. P. Gillis, "Fracture of Glass in Tensile and Bending Tests," *Metall. Mater. Trans. A*, **25A**, 961–7 (1994).
[34]G. R. Baran, "Fractal Characteristics of Fracture Surface," *J. Am. Ceram. Soc.*, **75** [10] 2687–91 (1992). □